Observer-oriented Thermal Modeling for Hall-Héroult Process

Taha Moncef Maouche, Andrea Mattioni, Lucas José da Silva Moreira, Hervé Roustan, Mirko Fiacchini, Gildas Besancon

Observer-oriented Thermal Modeling for Hall-Héroult Process

Taha Moncef Maouche * **Andrea Mattioni** **
Lucas José da Silva Moreira ** **Hervé Roustan** **
Mirko Fiacchini * **Gildas Besançon** *

* *Univ. Grenoble Alpes, CNRS, Grenoble INP, GIPSA-lab, Grenoble, France (e-mail: taha-moncef.maouche, mirko.fiacchini, gildas.besancon @grenoble-inp.fr).*
** *Rio Tinto, Laboratoire de Recherche de Fabrications, Saint-Jean-de-Maurienne, France (e-mail: andrea.mattioni, lucasjose.dasilvamoreira, herve.roustan @riotinto.com)*

Abstract: Temperature measurement is essential for the control of alumina dissolution and the stability of the cell in the Hall-Héroult process. However, the deployment of conventional sensors is a challenging task due to the corrosive nature of the process. In this paper, a zero-dimensional thermal model for real-time bath temperature estimation is proposed. A thermal model candidate for cell temperatures is constructed using alumina concentration estimations and available measurements. The thermal model is validated on industrial data.

Keywords: Hall-Héroult process, Alumina electrolysis, Thermal modeling, Industrial data.

1. INTRODUCTION

Hall-Héroult process is the main industrial method used for aluminum production (Grjotheim and Welch, 1988). This process consists in an electrochemical reaction generated by an electric current flowing in an electrolyte bath composed mainly of cryolite and dissolved alumina (Al_2O_3) (Bearne, 1999). The current separates the aluminum from oxygen forming a metallic liquid layer on the surface of the cathode while oxygen reacts with carbon anodes producing carbon dioxide gas (CO_2).

Unmeasured energy losses can be caused by irregular events such as anode change, reducing the overall performance of the cell. In addition, when dissolved alumina concentration reaches critical low levels, anode effects can be triggered releasing high levels of greenhouse gas emissions (Gao et al., 2022). Moreover, since the dissolution of alumina is partially governed by the thermal variations of the cell (Haverkamp and Welch, 1998), measuring the bath temperature is necessary to achieve optimal alumina regulation and to reduce heat losses.

However, the corrosive nature of the cryolite and the high level of the magnetic field generated by the large current intensity -in order of hundreds of kilo ampere- render the use of real-time thermocouples a challenging task (Jakobsen et al., 2001). In standard production plants, bath temperature measurements are carried-out manually at widely spaced time intervals. For this reason, model-based approaches are considered (Taylor et al., 1996), these methods allow the implementation of observer-based temperature sensors (Besançon, 2007). Finite-element thermal models have been proposed (Biedler, 2003; Lalancette et al., 2023). But, they are difficult to implement in real-time monitoring due to their high computational load. Reduced-order discretized models are considered instead (Cheung et al., 2015; Wong, 2022), though these algorithms do not take into account alumina concentration effect on the thermal behavior. Distributed temperature estimators have also been provided based on observer design (Wong et al., 2021; LeBreux et al., 2013). However, the proposed estimators require thermocouple measurements as an observer input for the correction step.

This study introduces an intermediate zero-dimensional thermal model of the alumina-electrolysis cell referred to as the IZDT-model. Designed with an observer-oriented framework, this approach enables real-time temperature estimation in future applications without requiring thermal input data. The IZDT-model is validated on industrial data provided by Laboratoire de Recherche des Fabrications (LRF) Saint-Jean-de-Maurienne, France. The proposed system takes into account available real-time measurements as well as alumina concentration estimates given by a predefined mass dissolution observer, called "MD-observer" (Mattioni et al., 2025). The model is designed with a minimum number of heat exchanges without losing the main thermal features of the cell.

This paper is organized as follow: in Section 2, the construction of the IZDT-model is explained. A validation test is presented and analyzed in Section 3. Section 4 concludes with a summary of our work and future perspectives.

2. INTERMEDIATE THERMAL MODEL

This section is dedicated to the description of the cell architecture, the design of the IZDT-model and the development of its state-space representation.

2.1 Model architecture

A simplified representation of the cell is given in Fig 1.

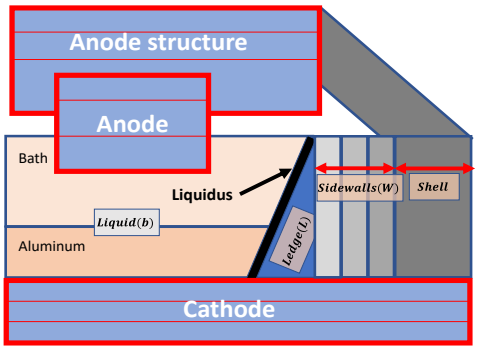

Fig. 1. Cross-sectional view of alumina-electrolysis cell

The system dynamics are derived by expressing the main heat exchanges between the cell structures. The cell can be decomposed into several elements with a core consisting of superposed layers of bath and metal located inside a rectangular pot. Multiple wall structures known as the sidewalls compose the pot. Due to the temperature difference between the liquid components and the sidewalls, a non-uniformly distributed frozen layer of cryolite known as ledge is formed on the surface of the sidewalls (Sanogo et al., 2024). The sidewalls are reinforced with a shell structure isolating the electrolysis cell from the ambient air. A portion of the heat is evacuated above and below the cell through anode and cathode structures, these structures are discretized into vertically superposed sub-blocks.

2.2 Hypotheses and simplifications

To achieve zero-dimensional thermal modeling of the cell, the following hypotheses are posed:

Hypothesis 1. The temperature of each block is assumed to be uniform and represented by a single node.

Hypothesis 2. Since the aluminum is an excellent thermal conductor, the liquid metal and the bath are considered as a single element block referred to as "liquid", with a single node temperature T_b.

Hypothesis 3. Cascaded sidewalls and shell are replaced by a single equivalent sidewall structure.

Hypothesis 4. The parallel anode blocks are replaced by a single anode structure with equivalent enthalpy.

Hypothesis 5. Ledge is considered to be uniformly distributed on the walls of the cell with an equivalent node temperature T_L.

2.3 State-space representation

Following the previous hypotheses, the overall cell can be visualized using the simplified block diagram in Fig 2.
The temperature derivative of each node k in Fig 2 can be expressed using the first principle of thermodynamics:

$$c_k \frac{d(m_k(t)T_k(t))}{dt} = Q_k(t) \tag{1}$$

where c_k, m_k, T_k, Q_k are respectively : the specific thermal capacity $[J/kg/K]$, the mass $[kg]$, the temperature $[K]$ and the sum of heat fluxes $[W]$ exchanged within node k with:

$$k \in [b, L, W, A, C]$$

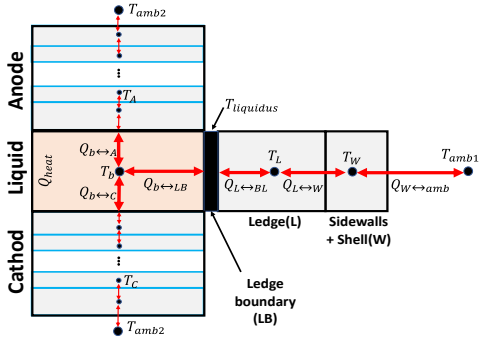

Fig. 2. Simplified diagram of the considered cell elements

where $[b, L, W, A, C]$ are the nodes associated respectively to the blocks: liquid, ledge, sidewall, A^{th} anode sub-block and C^{th} cathode sub-block.
The heat transfer between two connected nodes n and m is denoted by $Q_{n\leftrightarrow m}$.
The IZDT-model of the cell can then be constructed using the following ODEs:

$$\dot{T}_b(t) = \frac{1}{m_b(t)} \left(\frac{Q_b(t)}{c_b} - \dot{m}_b(t) T_b(t) \right) \tag{2a}$$

$$\dot{T}_L(t) = \frac{1}{m_L(t)} \left(\frac{Q_L(t)}{c_L} - \dot{m}_L(t) T_L(t) \right) \tag{2b}$$

$$\dot{T}_W(t) = \frac{Q_W(t)}{c_W m_W} \tag{2c}$$

where the terms Q_b, Q_L and Q_W are given by the following set of equations:

$$Q_b(t) = Q_{heat}(t) - Q_{b\leftrightarrow LB}(t) - Q_{b\leftrightarrow A}(t) - Q_{b\leftrightarrow C}(t) \tag{3a}$$

$$Q_L(t) = Q_{LB\leftrightarrow L}(t) - Q_{L\leftrightarrow W}(t) \tag{3b}$$

$$Q_W(t) = Q_{L\leftrightarrow W}(t) - Q_{W\leftrightarrow amb}(t) \tag{3c}$$

where Q_{heat} is the generated heat in the cell core. $Q_{b\leftrightarrow LB}$, $Q_{b\leftrightarrow A}, Q_{b\leftrightarrow C}, Q_{LB\leftrightarrow L}, Q_{L\leftrightarrow W}, Q_{W\leftrightarrow amb}$ are the heat transfers connecting respectively: liquid to ledge boundary, liquid to anode block, liquid to cathode block, ledge boundary to ledge, ledge to sidewall and sidewall to ambient air.
All of the listed heat terms are explained in Section 2.4.

2.4 Heat transfer terms

This section lists the main heat flux transfers between the different cell elements mentioned in equation (3).

Heat generation: The cell voltage generated from the line current flow can be separated into two terms: the first term is an electrochemistry term representing the electric potential needed for the chemical reaction, while the second term is the heating potential representing the heat dissipation in the cell core. The main source of the cell core heating comes from the Ohm's power law:

$$Q_{heat}(t) = V_{heat}(t) I_{line}(t) \tag{4}$$

where I_{line} is the line current and V_{heat} is the voltage used for the cell heating.
The heating voltage is given in terms of the measured pseudo-resistance of the cell R (Kvande et al., 2016):

$$V_{heat}(t) = I_{line}(t) R(t) + V_0 - V_{metal}(t) \tag{5}$$

where V_{metal} is the aluminum production voltage and V_0 is a fixed voltage set according to the cell's technology.

The pseudo-resistance R can be deduced from the cell voltage measurements V_{cell} (Haupin, 2016):

$$R(t) = \frac{V_{cell}(t) - V_0}{I_{line}(t)} \tag{6}$$

Replacing (5) in (4):

$$Q_{heat}(t) = (I_{line}(t)R(t) + V_0 - V_{metal}(t))I_{line}(t) \tag{7}$$

In order to remove noise disturbance when estimating the generated heat in (7), a filtered version of the pseudo-resistance $\hat{R}$ obtained from MD-observer can be used instead of the raw measured pseudo-resistance R. A filtered generated heat $\hat{Q}_{heat}$ can then be given by:

$$\hat{Q}_{heat}(t) = (I_{line}(t)\hat{R}(t) + V_0 - V_{metal}(t))I_{line}(t) \tag{8}$$

The power needed for metal production Q_{metal} given a mass rate of the produced aluminum $\dot{m}_{Al}$ can be described using the following expression:

$$Q_{metal}(t) = \dot{m}_{Al}(t)\Delta H_{Al} \tag{9}$$

where ΔH_{Al} is the enthalpy of metal production given in $[J/kg]$ and m_{Al} is the mass of the liquid aluminum.
Metal production power Q_{metal} can also be expressed as the product of metal production voltage and line current:

$$Q_{metal}(t) = V_{metal}(t)I_{line}(t) \tag{10}$$

The mass rate of aluminum $\dot{m}_{Al}$ is given by Faraday's law:

$$\dot{m}_{Al}(t) = \frac{xM_{Al}}{3\mathcal{F}}I_{line}(t) \tag{11}$$

where x is the current efficiency of the cell, M_{Al} is the aluminum molar mass, 3 is the valence number of aluminum and $\mathcal{F}$ is the Faraday constant.
By replacing (11) in (9):

$$Q_{metal}(t) = \Delta H_{Al}\frac{xM_{Al}}{3\mathcal{F}}I_{line}(t) \tag{12}$$

The obtained equation (12) can be used to identify the metal production voltage from (10):

$$V_{metal}(t) = \Delta H_{Al}\frac{xM_{Al}}{3\mathcal{F}} \tag{13}$$

The proposed term is an average estimation of the metal production voltage taking into account the average energy used for pre-heating alumina and anodes at a theoretical alumina feeding frequency.

Heat transfer from liquid to ledge: Liquid metal, liquid bath and frozen ledge have different phases. Therefore, heat is not directly transferred from the liquid to the ledge. In fact, the heat will be first transferred from the liquid to the liquid-ledge interface denoted as $Q_{b\leftrightarrow LB}$, and then, from liquid-ledge interface to the ledge $Q_{LB\leftrightarrow L}$. This interface is commonly known in the alumina-electrolysis field as the liquidus or the ledge boundary "LB".

Heat transfer from liquid to liquidus: This term represents the heat transfer at the surface intersection between the liquid and LB. The liquid to LB exchange term Q_{b-LB} is defined below by Newton's heat convection principle:

$$Q_{b\leftrightarrow LB}(t) = \Delta T(t)\left(h_{B-L}A_{B-L} + h_{m-L}A_{m-L}(t)\right) \tag{14}$$

where h_{B-L}, h_{m-L} are respectively the heat transfer coefficients from bath to ledge and from metal to ledge in $[W/m^2/K]$. The pair $(A_{B-L}; A_{m-L})$ is the exchange heat surfaces between bath-ledge and metal-ledge in $[m^2]$.
Both heat transfers from metal and bath to LB are summed up by Q_{b-LB}, where ΔT is the superheat given by the difference between the liquid temperature T_b and the liquidus temperature T_{liq} at the LB:

$$\Delta T(t) = T_b(t) - T_{liq}(t) \tag{15}$$

Several articles have discussed the identification process of the liquidus temperature using the superposition of the bath chemical components effect on the liquidus temperature difference. In this article, the liquidus expression from Solheim et al. (2016) has been chosen. The selected liquidus expression is highly sensitive to the concentrations of alumina and aluminum fluoride (AlF_3) commonly used for bath temperature regulation.
To compute superheat in real-time, the liquidus temperature must also be available in real-time. However, in practice, liquidus temperature is updated only when new alumina concentration samples are manually collected. As an alternative, liquidus temperature can be computed in real-time using alumina concentration estimations $\hat{w}_d$ provided by the MD-observer. The architecture of the modeling approach is shown in Fig 3.

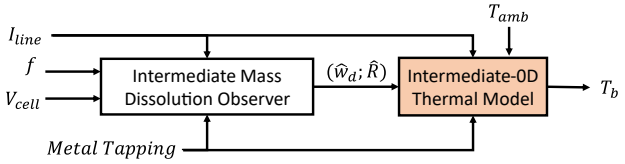

Fig. 3. Block diagram of the IZDT-model

The exchange surfaces A_{B-L} and A_{m-L} are given below:

$$A_{B-L} = 2(H_B(L_B + W_B)) \tag{16a}$$

$$A_{m-L}(t) = 2(H_m(t)(L_m + W_m)) \tag{16b}$$

where H, L, W are the height, length and width of each intersection surface.
The height of the bath H_B is fixed, whereas the height of the metal H_m is a function of the produced metal mass. Equation (11) can be adjusted to obtain the dynamic of the metal height:

$$\dot{H}_m(t) = \frac{xM_{Al}}{3\mathcal{F}\rho_{Al}L_mW_m}I_{line}(t) - T_{ap}(t) \tag{17}$$

where ρ_{Al} is the mass density of liquid aluminum $[kg/m^3]$. $T_{ap}(t)$ is the equivalent height rate of the metal tapping measured in $[m/s]$ and can be considered as one of the intermediate thermal model inputs.

Heat transfer from liquidus to ledge: The heat transfer between LB and center of the ledge $Q_{LB\leftrightarrow L}$ is governed by Fourier's heat conduction law:

$$Q_{LB\leftrightarrow L}(t) = K_LA_L(t) \times \frac{T_{liq}(t) - T_L(t)}{0.5 \times \gamma(t)} \tag{18}$$

with γ being the ledge thickness in $[m]$, K_L is the thermal conductivity of the ledge in $[W/m/K]$ and A_L is the uniform liquid-ledge surface interface obtained by summing up the terms from (16):

$$A_L(t) = A_{B-L} + A_{m-L}(t) \tag{19}$$

The term γ is divided by 2 in equation (18) since we are only interested in estimating the thermal resistance between LB and the center of the ledge.
The instantaneous ledge thickness can also be deduced

from the molten/frozen mass of ledge by applying Stefan's heat conservation law at LB:

$$\dot{m}_L(t) = \frac{Q_{LB\leftrightarrow L}(t) - Q_{b\leftrightarrow LB}(t)}{H_{fus}} \tag{20}$$

where H_{fus} is the heat fusion constant of the ledge $[J/kg]$. The ledge thickness γ is proportional to the mass m_L:

$$\gamma(t) = m_L(t)\frac{A_L(t)}{\rho_L} \tag{21}$$

with ρ_L the mass density of the ledge $[kg/m^3]$.
The varying liquid mass can also be obtained from (20) using the mass conservation principle:

$$\dot{m}_b(t) = -\dot{m}_L(t) \tag{22}$$

Equation (22) is used in the general ODE system (2).

Heat transfer to sidewalls: The heat evacuated through the sidewalls from the center of the ledge to the center of the equivalent sidewall $Q_{L\leftrightarrow W}$ is given by constant thermal resistances R_W and R_L:

$$Q_{L\leftrightarrow W}(t) = \frac{T_L(t) - T_W(t)}{R_W + R_L} \tag{23}$$

The first resistance term R_W is the equivalent resistance from the ledge-sidewall interface to the middle of the sidewall structure.
The second thermal resistance R_L is the equivalent resistance from the ledge-sidewall interface to the fixed center of the ledge $\gamma_{1/2}$ given by the initial condition $\gamma(0)$:

$$\gamma_{1/2} = \frac{\gamma(0)}{2} \tag{24}$$

Heat evacuation from cell to ambient air: Newton's convection law is applied to express the heat transfer from the wall structure to the ambient air Q_{W-amb}:

$$Q_{W\leftrightarrow amb}(t) = (T_W(t) - T_{amb1}(t))h_{w-amb}A_W \tag{25}$$

where the constant h_{w-amb} is the heat transfer coefficient between the cell external wall and the ambient air, and A_W is their exchange surface. $T_{amb1}(t)$ is the ambient temperature of the air in contact with the sidewall surface and can also be considered as a model input.

Heat evacuation through anode and cathode: Anode and cathode structures are composed of S sub-blocks, each sub-block i is discretized into N_i nodes.
The notations of this section are given in Appendix A.1.
The temperature derivative of each node T_j^i is given by the thermodynamic principle (1):

$$\dot{T}_j^i(t) = \frac{1}{C_j^i}\left(Q_{j-1\leftrightarrow j}^i - Q_{j\leftrightarrow j+1}^i + Q_{gen}^i(t)\right) \tag{26}$$

$$\dot{T}_j^i(t) = \frac{T_{j-1}^i(t) - T_j^i(t)}{C_j^i R_{j-1\leftrightarrow j}^i} - \frac{T_j^i(t) - T_{j+1}^i(t)}{C_j^i R_{j\leftrightarrow j+1}^i} + \frac{Q_{gen}^i(t)}{C_j^i} \tag{27}$$

for all $i \in [1..S]$ and $j \in [1..N_i]$.
where C_j^i, T_j^i are the heat capacity $[J/K]$ and the temperature $[K]$ of the j^{th} node of the i^{th} sub-block, while $R_{j\leftrightarrow j+1}^i$ is the thermal resistance connecting node j to its neighbor node $j+1$. Q_{gen}^i is the heat created by the line current passing through sub-block i and $Q_{j-1\leftrightarrow j}^i, Q_{j\leftrightarrow j+1}^i$ are the heat transfer terms between node j and its neighbor nodes $j-1$ and $j+1$.

The heat transfer between two adjacent sub-blocks is expressed using the following boundary condition:

$$\frac{T^{i\leftrightarrow i+1}(t) - T_1^{i+1}(t)}{R_1^{i\leftrightarrow i+1}} = \frac{T_{N_i}^i(t) - T^{i\leftrightarrow i+1}(t)}{R_{N_i}^{i\leftrightarrow i+1}} \tag{28}$$

where $T^{i\leftrightarrow i+1}$ is the interface temperature between sub-block i and its adjacent sub-block $i+1$. The node temperatures $T_{N_i}^i$ and T_1^{i+1} are connected to the interface temperature $T^{i\leftrightarrow i+1}$ with the equivalent thermal resistances: $R_{N_i}^{i\leftrightarrow i+1}$ and $R_1^{i\leftrightarrow i+1}$.

The same principle can be applied to determine the boundary conditions between the first sub-block of anode/cathode and the liquid, and between the last anode/cathode sub-block and the ambient air:

$$\frac{T_b(t) - T^{b\leftrightarrow 1}(t)}{R_b^{b\leftrightarrow 1}} = \frac{T^{b\leftrightarrow 1}(t) - T_1^1(t)}{R_1^{b\leftrightarrow 1}} \tag{29a}$$

$$\frac{T^{S\leftrightarrow amb2}(t) - T_{amb2}(t)}{R_{amb2}^{S\leftrightarrow amb2}} = \frac{T_{N_S}^S(t) - T^{S\leftrightarrow amb2}(t)}{R_{N_S}^{S\leftrightarrow amb2}} \tag{29b}$$

where $T^{b\leftrightarrow 1}$ is the interface temperature connecting the liquid to the first node of the first sub-block T_1^1 of either anode or cathode. The heat transfer between $T^{b\leftrightarrow 1}$ to the liquid and between $T^{b\leftrightarrow 1}$ to anode or cathode block are expressed respectively by the thermal resistances $R_1^{b\leftrightarrow 1}$ and $R_b^{b\leftrightarrow 1}$. Similarly, $T^{S\leftrightarrow amb2}$ is the interface temperature connecting ambient air temperature T_{amb2} to the last node N_S of the last sub-block S of either anode or cathode. The heat transfer between $T^{S\leftrightarrow amb2}$ to the ambient air and between $T^{S\leftrightarrow amb2}$ to anode or cathode block are given respectively by the resistances $R_{amb2}^{S\leftrightarrow amb2}$ and $R_{N_S}^{S\leftrightarrow amb2}$.
The exchange between liquid and anode/cathode mentioned in equation (3) can be determined from (29):

$$Q_{b\leftrightarrow A}(t) = \frac{T_b(t) - T^{b\leftrightarrow A1}(t)}{R_b^{b\leftrightarrow A1}} \tag{30a}$$

$$Q_{b\leftrightarrow C}(t) = \frac{T_b(t) - T^{b\leftrightarrow C1}(t)}{R_b^{b\leftrightarrow C1}} \tag{30b}$$

where $T^{b\leftrightarrow A1}, T^{b\leftrightarrow C1}$ are respectively the interface temperatures between liquid and first anode and first cathode sub-blocks with the equivalent thermal resistances $R_b^{b\leftrightarrow A1}$ and $R_b^{b\leftrightarrow C1}$ connecting the liquid to the first sub-blocks of anode and cathode.

3. RESULTS & VALIDATION

The cells studied in LRF are equipped with real-time bath temperature thermocouple. This sensor allows the validation of IZDT-model using real-time data.

3.1 Model initialization

In the beginning of the simulation or after the end of an event such as: metal tapping, anode change, anode effect or sensor disconnection, the bath temperature initial condition of the IZDT-model is set to the value of the thermocouple. As for the ledge and the sidewall states, the equilibrium states of (2) are used as their initial conditions:

$$Q_{b\leftrightarrow LB}(0) = \Delta T(0)(h_{B-L}A_{B-L} + h_{m-L}A_{m-L}(0)) \tag{31}$$

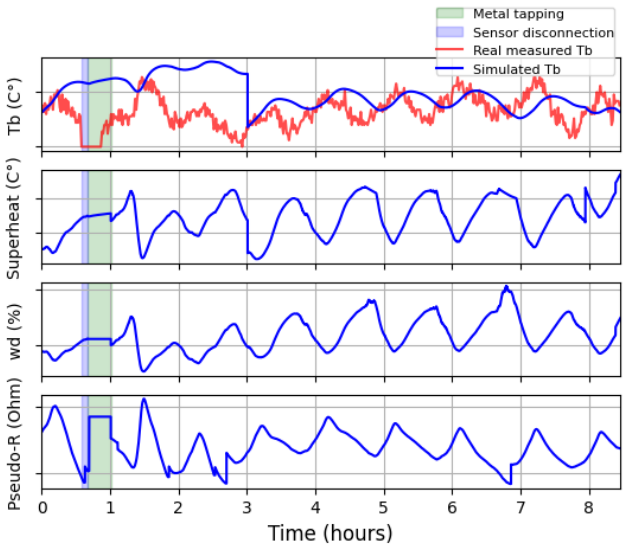

Fig. 4. Model validation on thermocouple data including metal tapping event in industrial plant

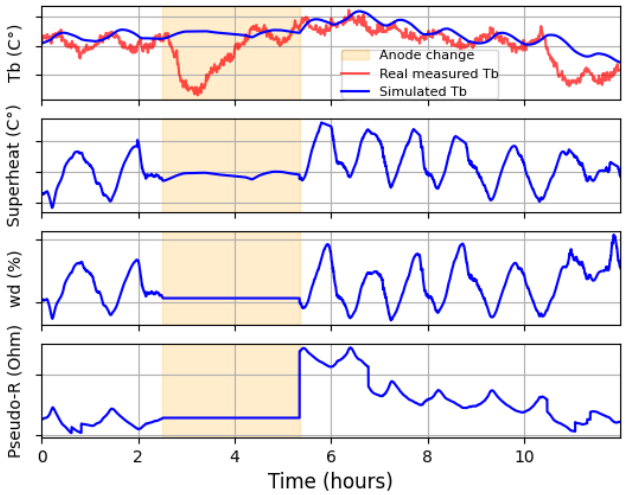

Fig. 5. Model validation on thermocouple data including anode change event in industrial plant

$$T_W(0) = \frac{Q_{b\leftrightarrow LB}(0)}{h_{w-amb}A_w} + T_{amb1}(0) \tag{32a}$$

$$T_L(0) = Q_{b\leftrightarrow LB}(0)(R_L + R_W) + T_W(0) \tag{32b}$$

$$\gamma(0) = \frac{2K_L A_L(0)(R_L + R_W)(T_{liq}(0) - T_L(0))}{T_L(0) - T_W(0)} \tag{32c}$$

The initial condition of liquidus temperature $T_{liq}(0)$ is computed using the initial condition of the estimated alumina concentration $\hat{w}_d(0)$ given by the MD-observer.

3.2 Model validation

Two validation tests are shown in Fig 4 and 5. In order to avoid model divergence due to unmeasured disturbances, simulation is reset within a fixed time window after the end of a detected event, this window allows the MD-observer to re-converge. The reset window is also used as a temporization for the cell's heat balance stabilization.
In Fig 4, an overshoot of the pseudo-resistance can be noticed after the end of a metal tapping event. Simultaneously, the superheat is estimated at high levels which explains the IZDT-model divergence from real bath temperature. When three hours of simulation have passed, the model is reset resulting into a more precise simulation. In the second simulation Fig 5, the IZDT model accurately reproduces the measured bath temperature following an anode change by leveraging the observed increase -before and after the event- in pseudo-resistance used in computing the core heating energy Q_{heat}. For both simulations, the IZDT-model matches the real thermocouple measurements during normal operational conditions with respective bath temperature RMS errors of $2.12°C$ and $1.96°C$.
The model is also capable of detecting derivative changes in temperature with slight delay between simulation and real measurements, this delay being caused by the approximation of the metal production enthalpy ΔH_{Al} which does not take into account the effect of the variable feeding frequency f. The bath temperature local minima and maxima correspond to the superheat high and low peaks. These peaks are directly related to the alumina concentration present in the bath, demonstrating that alumina dissolution energy has a direct impact on the bath temperature.

The repeatability of the results can be assessed by extending the simulations over a one-week trial period. The output error between simulated bath temperature and thermocouple measurement was evaluated. This test excluded special events mentioned in Section 3.1. The error distribution of the tests is shown in Fig 6.

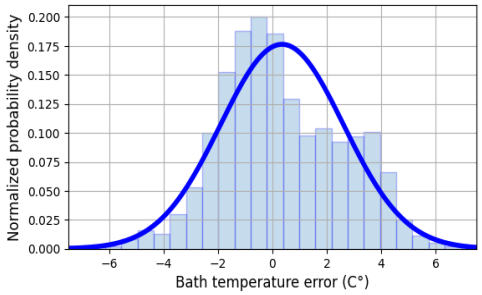

Fig. 6. Error density distribution of 7-day simulation tests

An RMS error of $2.23°C$ was obtained over the 7-days validation period. It is worth noting that achieving zero error is challenging due to the unmeasured heat losses. Additionally, the simulated temperature corresponds to an average bath temperature, whereas the thermocouple measurements are taken at the cell's extremity. Given the considered constraints and the resulting RMS error, the IZDT-model can be considered as a valid candidate for the design of bath temperature observer.

4. CONCLUSION

This paper proposes a zero-dimensional model for bath temperature, intended for observer design. It has been shown that the IZDT-model captures the key changes of alumina dissolution and resistance levels. The simulated temperature successfully matches real data satisfying validation phase despite the unmeasured thermal disturbances. In addition, the simulation reset condition succeeding irregular operations prevents the IZDT-model from diverging.

In the continuity of this work, different topics can be studied. The model can be improved by considering AlF_3 concentration and studying its effect on the liquidus temperature. The delay in the temperature response of the dynamical system can be further explored by integrating the variation of the feeding frequency f in the estimation of the enthalpy ΔH_{Al}. Finally, the IZDT-model can serve as an observer-design candidate for future work.

REFERENCES

Bearne, G.P. (1999). The development of aluminum reduction cell process control. *JOM*, 51(5), 16–22.

Besançon, G. (2007). *Nonlinear observers and applications*, volume 363. Springer.

Biedler, P. (2003). *Modeling of an aluminum reduction cell for the development of a state estimator*. West Virginia University.

Cheung, C.Y., Menictas, C., Bao, J., Skyllas-Kazacos, M., and Welch, B.J. (2015). Spatial thermal condition in aluminum reduction cells under influences of electrolyte flow. *Chemical Engineering Research and Design*, 100, 1–14.

Gao, B., Niu, H., Guan, Y., Wang, Z., Liu, J., Taylor, M.P., and Chen, J.J. (2022). Visualization of anode effect in aluminum electrolysis. *Journal of the Electrochemical Society*, 169(1), 013505.

Grjotheim, K. and Welch, B.J. (1988). Aluminium smelter technology–a pure and applied approach. *Aluminium-Verlag, P. O. Box 1207, Konigsallee 30, D 4000 Dusseldorf 1, FRG, 1988.*

Haupin, W. (2016). Interpreting the components of cell voltage. In *Essential Readings in Light Metals: Volume 2 Aluminum Reduction Technology*, 153–159. Springer.

Haverkamp, R.G. and Welch, B.J. (1998). Modelling the dissolution of alumina powder in cryolite. *Chemical Engineering and Processing: Process Intensification*, 37(2), 177–187.

Jakobsen, S.R., Hestetun, K., Hovd, M., and Solberg, I. (2001). Estimating alumina concentration distribution in aluminium electrolysis cells. *IFAC Proceedings Volumes*, 34(18), 303–308.

Kvande, H., Moxnes, B.P., Skaar, J., and Solli, P.A. (2016). Pseudo resistance curves for aluminium cell control-alumina dissolution and cell dynamics. In *Essential Readings in Light Metals: Volume 2 Aluminum Reduction Technology*, 760–766. Springer.

Lalancette, F., Désilets, M., Pansiot, B., LeBreux, M., and Bilodeau, J.F. (2023). Dimensional reduction of a 3d thermoelectric model to create a reliable and time-efficient 2d model representing an aluminum electrolysis cell. *International Journal of Heat and Mass Transfer*, 202, 123777.

LeBreux, M., Desilets, M., and Lacroix, M. (2013). An unscented kalman filter inverse heat transfer method for the prediction of the ledge thickness inside high-temperature metallurgical reactors. *International Journal of Heat and Mass Transfer*, 57(1), 265–273.

Mattioni, A., da Silva Moreira, L.J., Roustan, H., Fiacchini, M., and Besançon, G. (2025). Two-stage lumped parameter observer for spatial alumina concentration in aluminium reduction cells: Validation on simulator and industrial data. *Control Engineering Practice*, 165, 106525.

Sanogo, B., Dion, L., Gaboury, S., Kiss, L., Roger, T., Guérard, S., and Bilodeau, J.F. (2024). A review of challenges and solutions in ledge control and measurement in aluminium electrolysis cell. In *TMS Annual Meeting & Exhibition*, 577–585. Springer.

Solheim, A., Rolseth, S., Skybakmoen, E., Støen, L., Sterten, Å., and Støre, T. (2016). Liquidus temperature and alumina solubility in the system na3alf6-alf3-lif-caf2-mgf2. In *Essential Readings in Light Metals: Volume 2 Aluminum Reduction Technology*, 73–82. Springer.

Taylor, M., Zhang, W., Wills, V., and Schmid, S. (1996). A dynamic model for the energy balance of an electrolysis cell. *Chemical Engineering Research and Design*, 74(8), 913–933.

Wong, C.J. (2022). *Dynamic mass and heat balance model of hall-héroult cells: a discretised approach*. Ph.D. thesis, University of New South Wales (Australia).

Wong, C.J., Yao, Y., Bao, J., Skyllas-Kazacos, M., Welch, B.J., Jassim, A., and Mahmoud, M. (2021). Discretized thermal model of hall-héroult cells for monitoring and control. *IFAC-PapersOnLine*, 54(11), 67–72.

Appendix A. VARIABLES USED FOR ANODE & CATHODE MODELING

Table A.1. Symbol, description and unit of variables used in anode & cathode modeling

Symbol	Description	Unit
T^i_j	Temperature of j^{th} node of i^{th} sub-block	K
$T^{i\leftrightarrow i+1}$	Interface temperature between sub-block i and $i+1$	K
$T^{b\leftrightarrow 1}$	Interface temperature between liquid and 1^{st} anode or cathode sub-block	K
$T^{S\leftrightarrow amb2}$	Interface temperature between ambient air zone 2 and S^{th} anode or cathode sub-block	K
T_{amb2}	Ambient temperature of air zone 2	K
$R^i_{j-1\leftrightarrow j}$	Thermal resistance between nodes $j-1$ and j of sub-block i	$\frac{K}{W}$
$R_1^{i\leftrightarrow i+1}$	Thermal resistance between interface temperature $T^{i\leftrightarrow i+1}$ and sub-block $i+1$	$\frac{K}{W}$
$R_{N_i}^{i\leftrightarrow i+1}$	Thermal resistance between interface temperature $T^{i\leftrightarrow i+1}$ and sub-block i	$\frac{K}{W}$
$R_b^{b\leftrightarrow 1}$	Interface thermal resistance between liquid and interface temperature $T^{b\leftrightarrow 1}$	$\frac{K}{W}$
$R_1^{b\leftrightarrow 1}$	Interface thermal resistance between interface temperature $T^{b\leftrightarrow 1}$ and 1^{st} anode or cathode sub-block	$\frac{K}{W}$
$R_{N_S}^{S\leftrightarrow amb2}$	Interface thermal resistance between S^{th} anode or cathode sub-block and interface temperature $T^{S\leftrightarrow amb2}$	$\frac{K}{W}$
$R_{amb2}^{S\leftrightarrow amb2}$	Interface thermal resistance between interface temperature $T^{S\leftrightarrow amb2}$ and ambient air zone 2	$\frac{K}{W}$
$Q^i_{j-1\leftrightarrow j}$	Heat transfer between nodes $j-1$ and j of sub-block i	W
Q^i_{gen}	Heat generated in sub-block i	W
C^i_j	Heat capacity of node j of sub-block i	$\frac{J}{kg.K}$
$T^{b\leftrightarrow A1}$	Interface temperature between liquid and 1^{st} anode sub-block	K
$T^{b\leftrightarrow C1}$	Interface temperature between liquid and 1^{st} cathode sub-block	K